Mitochondrial ATP synthase is dispensable in blood-stage *Plasmodium berghei* rodent malaria but essential in the mosquito phase

Angelika Sturm, Vanessa Mollard, Anton Cozijnsen, Christopher D. Goodman, and Geoffrey I. McFadden[1]

Plant Cell Biology Research Centre, School of BioSciences, University of Melbourne, Melbourne, VIC 3010, Australia

Edited by John P. McCutcheon, University of Montana, Missoula, MT, and accepted by the Editorial Board February 18, 2015 (received for review December 15, 2014)

Mitochondrial ATP synthase is driven by chemiosmotic oxidation of pyruvate derived from glycolysis. Blood-stage malaria parasites eschew chemiosmosis, instead relying almost solely on glycolysis for their ATP generation, which begs the question of whether mitochondrial ATP synthase is necessary during the blood stage of the parasite life cycle. We knocked out the mitochondrial ATP synthase β subunit gene in the rodent malaria parasite, *Plasmodium berghei*, ablating the protein that converts ADP to ATP. Disruption of the β subunit gene of the ATP synthase only marginally reduced asexual blood-stage parasite growth but completely blocked mouse-to-mouse transmission via *Anopheles stephensi* mosquitoes. Parasites lacking the β subunit gene of the ATP synthase generated viable gametes that fuse and form ookinetes but cannot progress beyond this stage. Ookinetes lacking the β subunit gene of the ATP synthase had normal motility but were not viable in the mosquito midgut and never made oocysts or sporozoites, thereby abrogating transmission to naive mice via mosquito bite. We crossed the self-infertile ATP synthase β subunit knockout parasites with a male-deficient, self-infertile strain of *P. berghei*, which restored fertility and production of oocysts and sporozoites, which demonstrates that mitochondrial ATP synthase is essential for ongoing viability through the female, mitochondrion-carrying line of sexual reproduction in *P. berghei* malaria. Perturbation of ATP synthase completely blocks transmission to the mosquito vector and could potentially be targeted for disease control.

malaria | ATP synthase | ookinetes | mitochondrial endosymbiosis | aerobic respiration

The production of ATP by most eukaryotes occurs in two phases: (*i*) glycolysis, which oxidizes glucose into pyruvate; and (*ii*) oxidative phosphorylation or chemiosmosis, in which pyruvate is fully oxidized into carbon dioxide and water within the mitochondrion. During chemiosmosis, the mitochondrial respiratory chain generates a proton gradient that drives a rotary turbine, known as ATP synthase, located in the inner mitochondrial membrane. Chemiosmosis produces far more ATP than glycolysis but requires oxygen as a terminal electron acceptor.

Blood-stage malaria parasites scavenge glucose from the host via a glucose transporter (1) and feed it into their glycolysis pathway (2–6). However, despite having access to oxygen, asexual blood-stage malaria parasites do not undertake appreciable chemiosmosis (2–6). Rather, they perform what is termed aerobic glycolysis, converting 93% of scavenged glucose into lactate to supply their ATP (5). Aerobic glycolysis is favored by rapidly growing cells (e.g., yeasts, cancer cells, bloodstream trypanosomes, and blood-stage malaria parasites) because it can support faster growth than chemiosmosis (7, 8), the requirement for rapid growth apparently offsetting the low efficiency of glycolytic ATP production when glucose is abundant (7). Reduced chemiosmosis might also alleviate the production of reactive oxygen species, which could be problematic in conjunction with hemoglobin digestion practiced by blood-stage malaria parasites (9). Despite the almost total reliance on anaerobic glycolysis by asexual blood-stage malaria parasites, a small amount of electron transport activity within the mitochondrion is crucial to regenerate ubiquinone required as the electron acceptor for dihydroorotate dehydrogenase, an essential enzyme for pyrimidine biosynthesis (10), and probably to maintain a proton gradient for essential mitochondrial processes such as protein import.

Although the asexual blood-stage malaria parasites rely solely on aerobic glycolysis for energy generation, a small proportion of them undergo conversion to gametocytes, which execute a programmed remodeling of their central carbon metabolism (5). Gametocytes form in preparation for possible transmission to the insect phase of the life cycle should they be taken up in the blood meal of an anopheline mosquito. They are morphologically very distinct (11) and express different genes to asexual blood-stage parasites (12), and their mitochondrion enlarges and develops distinct cristae (which are lacking in asexual blood-stage parasite mitochondria) (2, 13–15). Gametocytes activate the tricarboxylic acid cycle, oxidizing glucose and also glutamate to prime their mitochondrial electron-transport chain (5).

Initially it was not clear whether malaria parasites had a canonical tricarboxylic acid cycle, electron-transport chain, or ATP synthase complex. Various components were either not identifiable or seemed to have been replaced by noncanonical substitutes (16–21). Nevertheless, the current consensus is that tricarboxylic acid cycling, electron transport, and ATP synthesis happen in the parasite mitochondrion, just not very much in asexual blood-stage parasites (16, 19, 22, 23). Indeed, genetic knockout studies have shown that components of the mitochondrial electron-transport chain are dispensable in blood-stage malaria parasites, so long as the ability to regenerate ubiquinone for pyrimidine synthesis is maintained (10, 24, 25). Electron transport-defective parasites exhibit a phenotype only in the insect stage, where they are unable to complete their development and cannot transmit back to a vertebrate (24, 25).

Mitochondrial ATP synthase harvests the proton gradient generated across the inner mitochondrial membrane by mitochondrial electron transport to phosphorylate ADP. ATP synthases comprise multiple subunits assembled into two domains: a membrane-integrated F_0 domain that generates rotation as a consequence of allowing protons to move down the gradient

This paper results from the Arthur M. Sackler Colloquium of the National Academy of Sciences, "Symbioses Becoming Permanent: The Origins and Evolutionary Trajectories of Organelles," held October 15–17, 2014 at the Arnold and Mabel Beckman Center of the National Academies of Sciences and Engineering in Irvine, CA. The complete program and video recordings of most presentations are available on the NAS website at www.nasonline.org/Symbioses.

Author contributions: A.S. and G.I.M. designed research; A.S., V.M., A.C., and C.D.G. performed research; and A.S. and G.I.M. wrote the paper.

The authors declare no conflict of interest.

This article is a PNAS Direct Submission. J.P.M. is a guest editor invited by the Editorial Board.

[1]To whom correspondence should be addressed. Email: gim@unimelb.edu.au.

This article contains supporting information online at www.pnas.org/lookup/suppl/doi:10.1073/pnas.1423959112/-/DCSupplemental.

across the membrane it occupies, and an extrinsic F_1 domain that catalyzes attachment of inorganic phosphate to ADP using rotation energy (26). The F_1 domain comprises α and β subunits, with the stoichiometry $\alpha_3\beta_3$, and the β subunit contains the catalytic center for ATP formation (26). Yeast null mutants for ATP synthase β subunit lose mitochondrial ATPase activity, grow well on glucose but poorly on glycerol, and still form the F_1 domain, albeit without a detectable β subunit (27, 28). To examine the role of ATP synthase in the life cycle of malaria parasites, we constructed a null mutant for the ATP synthase β subunit in the rodent malaria parasite *Plasmodium berghei*. We demonstrate that ATP synthase is not essential for blood-stage growth of the parasite. We describe the viability of the ATP synthase β subunit knockout parasites in mosquitoes and demonstrate that ATPase activity is essential for completion of the insect phase of the parasite life cycle.

Results

ATP Synthase β Subunit Gene of *P. berghei*. The PBANKA_145030 gene of *P. berghei* ANKA strain resides on chromosome 14, and the single exon encodes a protein of 533 amino acids; syntenic orthologs occur in all known *Plasmodium* spp. genomes (12). PBANKA_145030 contains Walker A and B motifs, an ATP binding site (29), and a C-terminal PFAM domain shared by all ATP synthase β subunits. A Clustal Omega multiple sequence alignment with the *Arabidopsis thaliana* and the mouse ATP synthase β subunit gene revealed large areas of conserved amino acid sequence (Fig. S1). The N terminus of the protein product of PBANKA_145030 is predicted to be a mitochondrial targeting peptide (Fig. S1) (30). We conclude that PBANKA_145030 encodes the mitochondrial ATP synthase β subunit (*Pb*ATPβ) in *P. berghei* rodent malaria parasites.

***Pb*ATPβ Is Targeted to the Mitochondrion and Expressed Throughout the Life Cycle.** To confirm the predicted mitochondrial localization of the *P. berghei* ATP synthase β subunit, we estimated that the first 240 nucleotides of the gene, which encode an N-terminal extension absent from the ATP synthase β subunit of *Escherichia coli* (AtpD), likely encoded a mitochondrial-targeting peptide. This sequence was fused to the gene encoding green fluorescent protein (GFP) driven by the constitutive promoter *Pb*EF1α. The resulting plasmid, called pL0017-$GFP_{\beta MITO}$ (Fig. 1*A*), was transfected into *P. berghei* blood stages, giving rise to the *Pb*βL-GFP parasite line. Transfectants accumulated GFP in a subcellular compartment also positive for the mitochondrial dye Rhodamine 123 (Fig. 1*B*). The GFP/Rhodamine 123-positive structures exhibit the typical morphology of mitochondria in asexual (31) and sexual (32) blood cell life-cycle stages of malaria parasites. To observe mitochondrial morphology in insect stages of *P. berghei*, *Anopheles stephensi* mosquitoes were fed on mice infected with *Pb*βL-GFP parasites, and oocyst development was observed and imaged at different days after infection. Seven days postinfection, the oocysts contained an extensively branched GFP-positive structure, which became increasingly branched with time and even developed lasso-like loops (Fig. 1*C* and Movies S1 and S2). After 22 d, we detected sporozoites in the mosquito salivary glands showing a single GFP-positive structure (Fig. 1*D*).

Transcriptome and proteome studies show that *Pb*ATPβ is expressed throughout the life cycle (12), and we used reverse transcriptase PCR to detect transcripts of *Pb*ATPβ in both asexual and sexual stages of the red-blood cell cycle, in oocysts and sporozoites of the mosquito stages, and throughout the liver stage (Fig. S2).

Genetic Knockout of the *Pb*ATPβ Gene and Abrogation of the *Pb*ATPβ Protein. The gene encoding *Pb*ATPβ in *P. berghei* was interrupted by double cross-over homologous recombination to introduce a selectable marker, human dihydrofolate reductase, in the middle of the coding sequence to delete the catalytic site (Fig. 2*A*). Pyrimethamine-resistant *P. berghei* appeared in blood smears 10 d after i.v. injection of electroporated parasites. A clonal line was recovered by limiting dilution and inoculation into 10 mice.

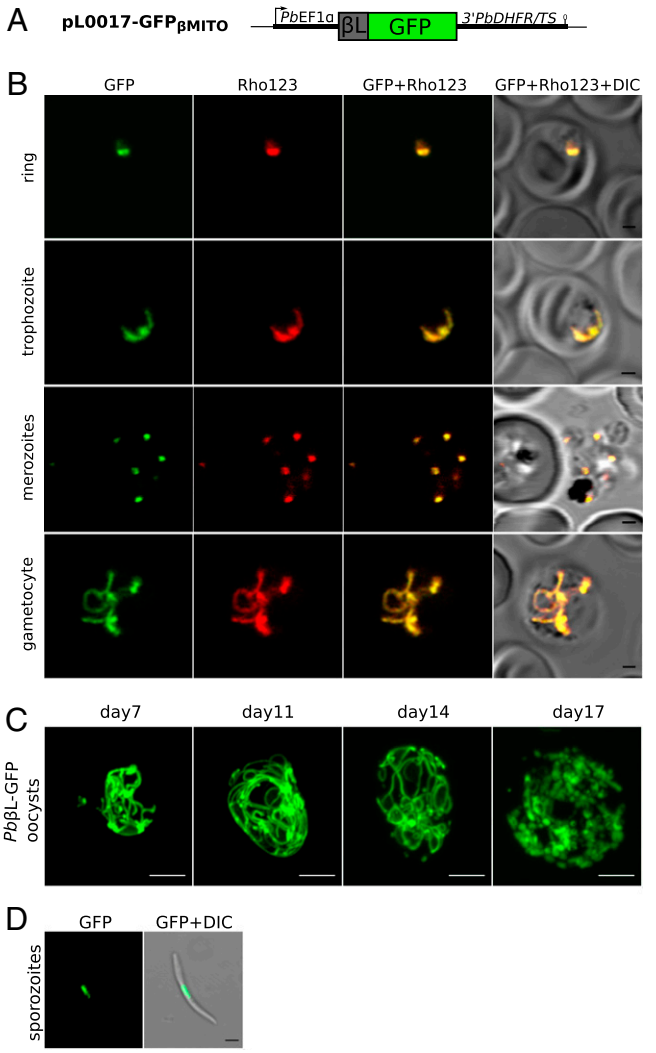

Fig. 1. The N-terminal extension of *Pb*ATPβ is a mitochondrion-targeting leader. (*A*) Construct (pL0017-$GFP_{\beta MITO}$) in which the first 80 codons from *Pb*ATPβ (βL) were fused to green fluorescent protein (GFP) and expressed under the constitutive *Pb*EF1α promoter. (*B*) Blood-stage parasites transfected with pL0017-$GFP_{\beta MITO}$ (*Pb*βL-GFP) expressing GFP (green) colocalized with the mitochondrial marker Rhodamine123 (Rho123, red). (Scale bar: 1 μm.) (*C*) Oocysts of *Pb*βL-GFP parasites on mosquito midguts at days 7, 11, and 14 after mosquito infection showing GFP fluorescence of the intricately branched mitochondrion. At day 17 after infection, the mitochondrion is dividing in preparation to provide each sporozoite with a single mitochondrion. (Scale bar, 5 μm.) (*D*) A sporozoite of the *Pb*βL-GFP line showing a single GFP-labeled mitochondrion in the mid region. (Scale bar: 1 μm.)

Clone $C6_I$ was used for further analysis and is hereafter referred to as *Pb*ATPβKO. Southern blotting using the 5′ integration sequence of the pL-βKO construct (Fig. 3*A*) as a probe confirmed integration of the selectable marker into the intended site (Fig. 3*B*). Western blotting using the commercial AtpB (beta subunit of ATP synthase) antiserum raised against a peptide conserved in the ATP synthase β subunit of plants, bacteria, and animals identified two bands. Uninfected mouse blood showed a band with an apparent mass of 50 kDa (Fig. 2*C*, *Upper*, lane 1), in close agreement with the predicted mass (excluding the predicted mitochondrial transit peptide of 5.98 kDa) (Fig. S1) of 50.3 kDa for mouse mitochondrial ATP synthase β subunit. In protein samples from mouse blood infected with the *P. berghei* ANKA WT parental line, a second, larger band of 54 kDa was identified, which is in good agreement with the predicted mass

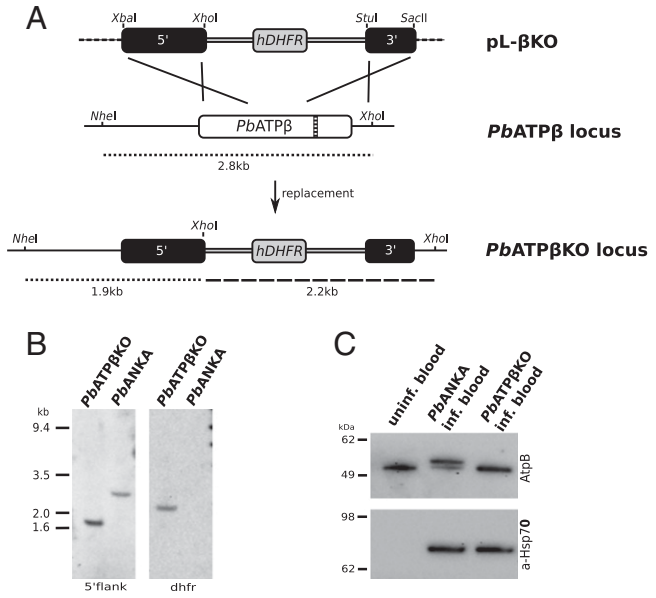

Fig. 2. Disruption of the *Pb*ATPβ gene locus to generate the *Pb*ATPβKO line, which lacks *Pb*ATPβ protein production. (*A*) The plasmid pL-βKO with a selectable marker (*h*DHFR) flanked by 5′ and 3′ integration sequences amplified from the *Pb*ATPβ gene locus (5′ and 3′ black boxes) undergoes double cross-over, homologous recombination to delete a large section of the gene, including the catalytic domain (hatched bar) of *Pb*ATPβ. (*B*) Southern blot of genomic DNA from the *Pb*ATPβKO cloned line and the *Pb*ANKA parental line digested with NheI and XhoI and probed with the 5′ integration sequence (5′ flank) showing a single 1.9-kb band for *Pb*ATPβKO and the expected 2.8-kb band for parental WT parasites (*Pb*ANKA). Probing the same DNA with an *h*DHFR probe (dhfr) shows the expected single band at 2.2 kb and no band for *Pb*ANKA. (*C*) Western blot of uninfected mouse blood, *Pb*ANKA-infected mouse blood, and *Pb*ATPβKO-infected mouse blood, probed with the generic ATPβ protein antibody AtpB (*Upper*). The mouse ATPβ protein (50.3 kDa, excluding predicted mitochondrial targeting sequence) is visible in uninfected mouse blood. A second, higher molecular mass band (53.5 kDa, excluding predicted mitochondrial targeting sequence) is visible in mouse blood infected with WT parasites but not mouse blood infected with *Pb*ATPβKO parasites. (*Lower*) A *P. berghei* loading control, in which the same membrane was probed with an a-Hsp70 antiserum showing clear bands for *Pb*Hsp70 (75 kDa) in *PbANKA*-infected mouse blood, as well as *Pb*ATPβKO-infected mouse blood. The Hsp70 does not recognize uninfected mouse blood.

(excluding the predicted mitochondrial transit peptide of 4.41 kDa) (Fig. S1) of 53.5 kDa for *Pb*ATPβ protein (Fig. 2*C*, lane 2). Mouse blood infected with *Pb*ATPβKO lacks the larger, parasite-specific band (Fig. 2*C*, *Upper*, lane 3). As a control for the presence of parasite material in *Pb*ATPβKO-infected blood, the same Western blot was probed with as anti-Hsp70 antibody raised against the *P. berghei* Hsp70 (Fig. 2*C*, *Lower*, lane 3). A second, independent knockout parasite line (*Pb*ATPβKO-YFP) was generated in a similar way to the *Pb*ATPβKO line, and Southern blotting showed deletion of the *Pb*ATPβ coding sequence and abrogation of protein production (Fig. S3).

***Pb*ATPβKO Parasites Have Slightly Impaired Growth During Blood Stage.** Growth of *Pb*ATPβKO in blood stage was compared with the parental line *Pb*ANKA (Fig. 3). For each line, two mice were i.v. injected with 1×10^5 asexual blood stages and then parasitemia and gametocytemia were measured by microscopy from day 1 to day 6 after infection. Growth comparison of WT and knockout parasites in two mice was repeated three times. Parasites were first seen 3 d after infection, which is shown as the first time point in the growth curves (Fig. 3 *A* and *B*). *Pb*ATPβKO grew slower (Fig. 3*A*) and produced fewer gametocytes (Fig. 3*B*), but the difference was not statistically significant. Generation of male gametes (exflagellation events) was counted for parental and knockout lines on days 4, 5, and 6 after infection. Male *Pb*ATPβKO gametocytes seemed to exflagellate normally and their sperm swam vigorously and bound multiple red blood cells, agglutinating erythrocytes similar to WT microgametes (Movie S3). *Pb*ATPβKO produced fewer exflagellations than the parent line, but this difference was not statistically significant (Fig. 3*C*).

Although the asexual growth of *Pb*ATPβKO was slower than the parental line when measured in separate mice, the difference was not statistically significant (Fig. 3*A*). Subtle growth deficiencies between parasites hosted by separate mice are difficult to substantiate so we decided to run coinfection trials with lines expressing different fluorophores. To represent the WT, we used *Pb*GFP$_{CON}$, which expresses green fluorescent protein and grows at normal blood-stage rates (33). We then created a red fluorescent version of the *Pb*ATPβKO line (*Pb*ATPβKO-G6Tm, expressing the tdTomato protein), which has an equivalent phenotype to our other two *Pb*ATPβ knockout lines (Table 1). We coinfected eight mice with equal numbers of both lines and counted parasitemias by flow cytometry on days 3 through 7 (Fig. 3*D*). In this growth competition experiment, it was clear that the *Pb*ATPβKO-G6Tm were substantially outgrown by the *Pb*GFP$_{CON}$ parasites from day 4 postinfection, almost disappearing by day 7 (Fig. 3*D*).

***Pb*ATPβKO Parasite Mitochondria Develop a Proton Gradient and Normal Morphology.** The mitochondria of both the asexual and sexual stages of *Pb*ATPβKO parasites accumulate Rhodamine 123 (Fig. 4*A*), a vital dye incorporated into mitochondria with a proton gradient. Transmission electron microscopy revealed that mitochondria of *Pb*ATPβKO asexual blood-stage parasites and gametocytes are indistinguishable from the parental line, having a canonical double membrane, granular contents, and distinct tubular cristae in gametocytes (Fig. 4*B*).

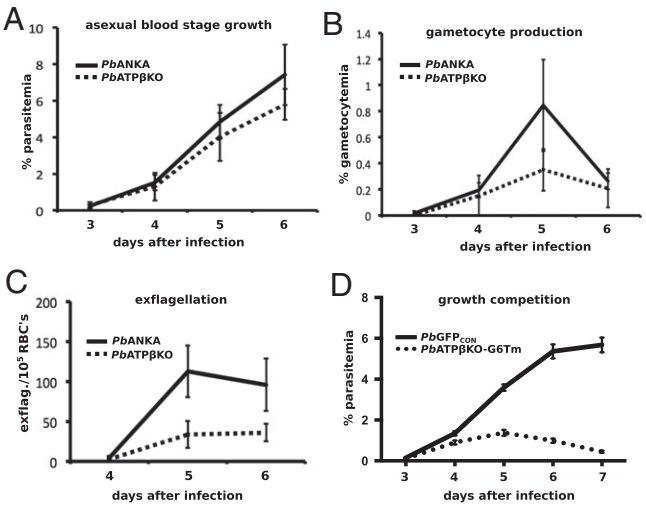

Fig. 3. Growth of *Pb*ATPβKO blood-stage parasites shows no significant difference to the parental line. (*A*) Blood-stage parasites of *Pb*ANKA and *Pb*ATPβKO were counted, and the parasitemia was determined at days 3–6 after i.v. injection of 1×10^5 asexual blood-stage parasites. At day 6 after infection, the difference in parasitemias is nonsignificant ($P = 0.25$, paired *t* test). (*B*) Gametocytes were counted at days 3–6 after infection from the same mice. No significant difference between gametocytemias was observed ($P = 0.31$, paired *t* test, at day 5 after infection). (*C*) Exflagellations per 1×10^5 red blood cells (RBCs) for *Pb*ANKA and *Pb*ATPβKO at days 4, 5, and 6 after infection were also determined for the same mice, and again no significant differences were found ($P = 0.09$, paired *t* test, at day 5 after infection). (*D*) Growth competition experiment using *Pb*ATPβKO-G6Tm and *Pb*GFP$_{CON}$ as the WT control. Parasites (5×10^4) of each line were i.v. injected into eight mice, and individual parasitemias were determined by FACS analysis between day 3 and day 7 after infection. The differences at days 4, 5, and 7 after infection are highly significant with a *P* value of <0.01 (multiple *t* test).

Table 1. Production of oocysts and sporozoites by self-fertilization or crossing of different lines of *P. berghei*

Parasite lines	No. of exps. done	Median no. of oocysts (range); *n* = no. of mosquitoes	Average no. of sporozoites per mosquito; *n* = no. of mosquitoes
*Pb*ANKA WT	3	77 (4–345); *n* = 37	9,950; *n* = 25
*Pb*ATPβKO	6	0; *n* = 60	0; *n* = 60
*Pb*ATPβKO-YFP	4	0; *n* = 26	0; *n* = 20
*Pb*ATPβKO-GTm	2	0; *n* = 30	0; *n* = 20
*Pb*ATPβKO (in vitro)	4	0; *n* = 50	4; *n* = 50
*Pbs*48/45KO	2	0; *n* = 17	300; *n* = 15
*Pb*ATPβKO: *Pbs*48/45KO	2	3 (0–45); *n* = 21	2,650; *n* = 15
Pbnek-4^{-}	3	0; *n* = 30	0; *n* = 30
*Pb*ATPβKO: *Pbnek-4*$^{-}$	3	0; *n* = 30	0; *n* = 30

*Pb*ATPβKO, PbATPβKO-YFP, and *Pb*ATPβKO-G6Tm parasites do not produce oocysts or sporozoites, but, when crossed with the male-infertile line *Pbs*48/45KO, fertility is restored. Mosquitoes were infected with individual *P. berghei* parasite lines or crosses of two lines, and, after 12 d, midgut oocysts were counted. Numbers represent the median number of oocysts per midgut, and the range in oocyst numbers per midgut is shown in parentheses. After 22 d, salivary-gland sporozoites were pooled and counted for each infection. Numbers represent the average sporozoite number per mosquito. *n* = number of mosquitoes dissected.

***Pb*ATPβKO Ookinetes Are Sensitive to the Mosquito-Gut Environment.** To monitor the ability of *Pb*ATPβKO gametocytes to mature and generate ookinetes, we harvested infected blood and transferred it to ookinete in vitro culture. After 22 h, we stained with an anti-Pbs28 antibody, a protein specific for activated females, zygotes, and ookinetes (Fig. 5*A*) (34). These developmental stages were subsequently counted and compared with a *P. berghei* ANKA WT control (Fig. 5*B*). Pbs28 staining does not distinguish activated females from recently fertilized, still-spherical zygotes, but, for the purpose of this experiment, the number of spherical zygotes was considered negligible. In vitro, we observed comparable activation of females and production of zygotes, and a slight, but significant (P value < 0.001) decrease in ookinete conversion rates for *Pb*ATPβKO in comparison with the parental *Pb*ANKA line (Fig. 5*B*).

To compare ookinete development in vivo, we allowed *A. stephensi* mosquitoes to bite mice infected with *Pb*ATPβKO. Twenty-two hours after feeding, the blood meal was removed from mosquitoes, stained with either Giemsa or anti-Pbs28, and activated females, zygotes, ookinetes and aberrant females were counted (Fig. 5*C*). In vivo development of gametocytes was drastically different from their development in vitro. The proportion of *Pb*ATPβKO activated females was substantially reduced in vivo (under 2%) compared with the parental *Pb*ANKA line (40%) (Fig. 5*C*). Similarly, the *Pb*ATPβKO line generated far fewer zygotes (0%) and ookinetes (0%) in vivo. Failure to activate, generate zygotes, and mature to ookinetes by the *Pb*ATPβKO female gametocytes in vivo was also evident in the preponderance of aberrant females in vivo (90%) compared with in vitro (1%) (Fig. 5 *B* and *C*, last columns). We did not observe any ookinetes in vivo at 22 h by Giemsa staining for *Pb*ATPβKO, but they were abundant in *Pb*ANKA.

The disparity between ookinete generation in vitro and in vivo by the *Pb*ATPβKO parasites was indicative of a viability problem in vivo. To hone in closer on where the *Pb*ATPβKO parasites incur this loss of ookinete viability, we performed a rescue experiment, transferring in vivo developing parasites to an in vitro situation at intervals. Mosquitoes were fed with either *Pb*ATPβKO or *P. berghei* ANKA-infected mice, and, after 5 or 10 h, their blood meals were dissected out and transferred to in vitro culture to continue their development for a total of 22 h. Removing the parasite from the midgut allowed us to visualize the impact of differing periods of midgut exposure on ookinete viability. After 5 h in the midgut, the *Pb*ATPβKO parasites went on to generate ookinetes in vitro (Fig. 5*D*). However, leaving the *Pb*ATPβKO parasites inside the mosquito gut for 10 h resulted in the production of a few early zygotes, but no ookinetes at the end of the subsequent 12 h in vitro incubation (Fig. 5*D*). We attempted to count activated females, zygotes, and ookinetes in these rescue experiments, but numbers were too inconsistent for comparison. Nevertheless, the rescue experiments reconcile the different success of ookinete production in vitro and in vivo, suggesting that ookinete production and/or viability in vivo is compromised by the lack of *Pb*ATPβ protein.

***Pb*ATPβKO Fails to Infect Mosquitoes.** Successful mosquito infection can be measured by counting oocysts, the sporozoite-producing parasite stage that develops from ookinetes able to exit the insect gut and develop in the hemocoel. We counted oocysts on midguts from mosquitoes infected with either the parental or *Pb*ATPβKO lines at day 12. No oocysts were observed on midguts of 60 *Pb*ATPβKO-fed mosquitoes from six independent infections (Table 1). Similarly, no oocysts were found in 26 *Pb*ATPβKO-YFP-fed mosquitoes from four independent infections (Table 1). By contrast, three independent infections with the *P. berghei* ANKA parental line led to the development of a median of 77 oocysts per midgut in 37 mosquitoes examined (Table 1). Accordingly, no sporozoites were detectable in the salivary glands of 60 *Pb*ATPβKO-fed mosquitoes or 20 *Pb*ATPβKO-YFP-fed mosquitoes after 22 d whereas *P. berghei* ANKA parental line-fed mosquitoes harbored an average of almost 10,000 sporozoites per set of mosquito salivary glands after 22 d (Table 1).

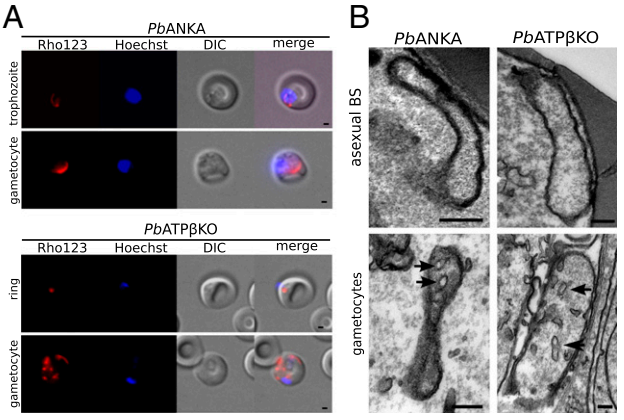

Fig. 4. Blood-stage *Pb*ATPβKO parasites have morphologically normal mitochondria that develop a proton gradient. (*A*) Parental WT (*Pb*ANKA) and *Pb*ATPβKO asexual blood-stage parasites labeled with the mitochondrial proton gradient dye Rhodamine123 (Rho123) showing morphologically normal mitochondria with intact proton gradients in knockout parasites lacking the *Pb*ATPβ protein. (Scale bar: 1 μm.) (*B*) Electron micrograph of *Pb*ANKA and *Pb*ATPKβO asexual and gametocyte mitochondria showing double membrane, granular contents, and cristae (black arrows) in gametocytes. BS, blood stage. (Scale bars: 0.2 μm.)

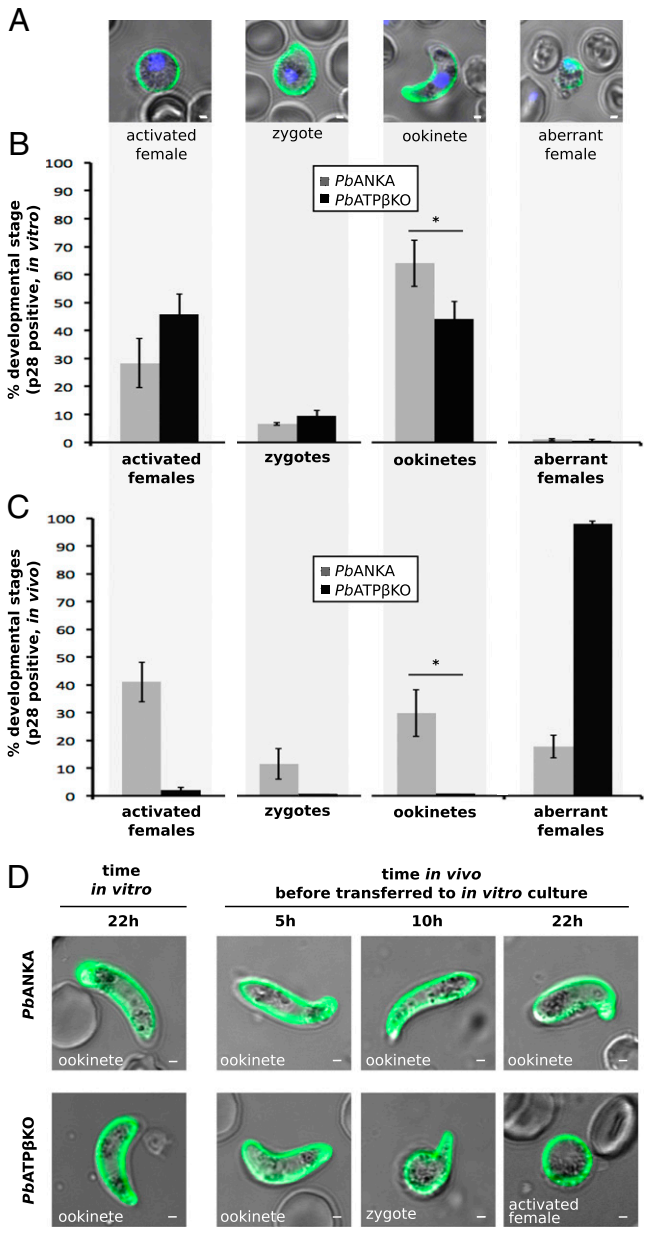

Fig. 5. *Pb*ATPβKO produces ookinetes in vitro, but not in vivo. Removing *Pb*ATPβKO-infected blood from the midgut leads to a partial rescue of the phenotype. (*A*) Anti-Pbs28 live immunolabeling (green) of *Pb*ATPβKO- and *Pb*ANKA-infected blood showing the four different developmental stages (activated females, zygotes, ookinetes, and aberrant females) present. DAPI staining shows parasite DNA (blue). (Scale bars: 1 μm.) (*B*) Percent composition of the four anti-Pbs28–labeled parasite stages present in in vitro cultures of *Pb*ANKA (gray) and *Pb*ATPβKO (black). The difference in ookinete conversion rate is statistically significant (**P* value < 0.01, Fisher's exact test). Error bars show SEM. (*C*) Percent composition of the four anti-Pbs28–labeled parasite stages present in in vivo blood meals of *Pb*ANKA-fed (gray) and *Pb*ATPβKO-fed (black) mosquitoes. **P* value < 0.01 (Fisher's exact test). Error bars show SEM. (*D*) Anti-Pbs28–labeled (green) cultures of *Pb*ANKA and *Pb*ATPβKO either cultured in vitro for 22 h or rescued into in vitro culture after 5, 10, or 22 h in vivo. *Pb*ANKA parasites developed into ookinetes under all circumstances, but *Pb*ATPβKO parasites failed to form ookinetes after as little as 10 h in vivo and seemed stalled at either zygote or activated female stage. (Scale bars: 1 μm.)

Mosquitoes fed on either the *P. berghei* ANKA parental line or *Pb*ATPβKO were held for 22 d to develop potential infections and then allowed to bite naive mice, which were subsequently tested for blood-stage patency from day 5 post-bite. No blood-stage parasites were observed after 20 d in three mice bitten by three different batches of *Pb*ATPβKO-infected and *Pb*ATPβKO-YFP–infected mosquitoes, which is consistent with the lack of oocysts or sporozoites (Table 1). As expected, all of the three mice bitten by mosquitoes infected with the *Pb*ANKA parental line developed blood-stage parasites between 6 and 8 d post-bite (Table 1).

The lack of oocyst and sporozoite production of the *Pb*ATPβKO parasite line (Table 1) is consistent with our observation that this knockout line fails to produce viable ookinetes in vivo (Fig. 5*C*). We wondered whether the in vitro-produced *Pb*ATPβKO ookinetes, which develop almost as successfully as WT ookinetes in this artificial environment (Fig. 5*B*), might successfully infect mosquitoes. *Pb*ATPβKO in vitro ookinetes were artificially fed to mosquitoes, and, after 12 d, midguts were checked for oocysts. In 50 mosquitoes from four independent feeds, no oocysts were found (Table 1). Accordingly, no sporozoites were observed 22 d after the feeds. Mosquitoes were allowed to feed on three mice, and, as expected, none of these mice had developed blood stages 20 d later.

***Pb*ATPβKO Ookinetes Glide with Normal Velocity.** Ookinetes glide in a corkscrew pattern through the blood meal to escape the mosquito midgut as rapidly as possible (35). We generated ookinetes from *Pb*ATPβKO parasites and a fluorophore expressing line *Pb*GFP$_{CON}$ in vitro, embedded them in a common matrix, and measured their gliding velocity by video microscopy (35, 36). Both the GFP-positive (WT) ookinetes and the *Pb*ATPβKO ookinetes (GFP-negative) glided at an equivalent average velocity of 4 μm·min^{-1} (Fig. 6), which is normal (35).

***Pb*ATPβKO Can Complement a Male-Deficient Parasite Line but Not a Female-Deficient Line.** The in vivo phenotype of *Pb*ATPβKO is indicative of a defect in the female gamete activation that is also manifest in the failure to produce robust zygotes and ookinetes. Given that mitochondria are inherited maternally in malaria parasites (32, 37, 38), we wondered whether the female gametes of *Pb*ATPβKO, whose mitochondrion has a nonfunctional ATP synthase, were ultimately unviable. To test this hypothesis, we performed crosses between *Pb*ATPβKO and *P. berghei* lines deficient in producing either viable male or female gametes, respectively (Fig. 6). *Pbs*48/45KO parasites have defective microgametes and severely reduced self-fertility (39). If *Pb*ATPβKO has defective macrogametes but viable microgametes, crossing it to male-deficient *Pbs*48/45KO should result in complementation and restoration of fertility (Fig. S4). When mice coinfected with *Pb*ATPβKO and *Pbs*48/45KO by i.v. injection of 2.5×10^5 parasites of each parasite line were fed to mosquitoes, we observed ookinetes in the mosquito gut 1 d after feeding, oocysts in the mosquito midguts after 12 d, and sporozoites in the salivary glands as early as 16 d postinfection (Table 1). Infecting naive mice with these sporozoites, either by mosquito bite or i.v. injection, led to blood-stage parasites in these mice within the expected timeframe.

To confirm that *Pb*ATPβKO has a defect in the female gamete, we crossed *Pb*ATPβKO with *Pbnek-4*$^-$, a line with abrogated female gamete viability (40). *Pbnek-4*$^-$ produces no ookinetes when self-fertilized, but fertility is largely restored when *Pbnek-4*$^-$ is crossed with a female-fertile line (40). If *Pb*ATPβKO parasites do not produce viable female gametes, they will not be able to complement *Pbnek-4*$^-$. Dual infected mice (*Pb*ATPβKO and *Pbnek-4*$^-$) were used to feed mosquitoes and midgut oocysts counted 12 d post-bite. As predicted, the *Pb*ATPβKO:*Pbnek-4*$^-$ cross produced no oocysts whereas a parallel self-fertilization experiment with *P. berghei* ANKA WT strain yielded the expected oocyst numbers (Table 1).

Discussion

Although malaria parasites generate most of their ATP via aerobic glycolysis during the blood stage of their life cycle, they appear to possess a complete ATP synthase complex and machinery to drive ATP production through complete glucose catabolism using oxygen as the ultimate electron acceptor, which

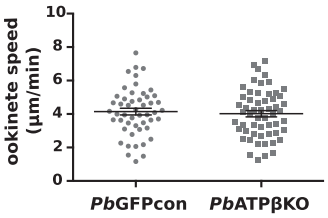

Fig. 6. Gliding velocity in $\mu m \cdot min^{-1}$ of ookinetes from WT ($PbGFP_{CON}$) and knockout parasites (*Pb*ATPβKO) showing no difference in average velocity. The wide bars represent average velocity, and the narrow bars show the SEM.

suggests that mitochondrial ATP synthase is active at other stages of the life cycle, either in the insect and/or the mammalian liver stage that precedes the blood stage. We took a reverse genetic approach to address this question and sought to knock out mitochondrial ATP synthase function in asexual blood-stage rodent malaria parasites and then phenotype the null mutant in sexual and proliferative stages of the life cycle in mosquitoes.

We characterized the gene for the β subunit of ATP synthase (*Pb*ATPβ) in the rodent malaria parasite *P. berghei*. We showed that the N terminus of the *Pb*ATPβ protein is a mitochondrial targeting peptide and that the protein has sequence features identifying it as the catalytic subunit of the ATP synthase complex. *Pb*ATPβ transcripts were detected throughout the entire life cycle, and *Pb*ATPβ protein was shown to be present in blood-stage parasites, consistent with previous expression analyses (12, 41, 42). Nevertheless, we successfully deleted most of the coding region of *Pb*ATPβ by targeting blood-stage, asexual parasites. Southern blots indicated a single insertion of the selectable marker at the target locus, removing the catalytic site responsible for phosphorylation of ADP. Western blotting demonstrated that the *Pb*ATPβKO parasites had no detectable *Pb*ATPβ protein, and we conclude that these parasites lack mitochondrial ATP synthase capacity.

Blood-stage, asexual rodent malaria parasites lacking *Pb*ATPβ grew marginally slower than WT, confirming that the bulk of parasite energetics is reliant on aerobic glycolysis at this life stage (2–5). Previous attempts to knock out the β subunit or γ subunit of mitochondrial ATP synthase in human malaria parasites, *Plasmodium falciparum*, were unsuccessful (16). This difference between *P. falciparum* and *P. berghei* could mean that human and rodent malaria parasites have very distinct requirements for ATP synthase during the asexual blood phase. However, there are no robust tools to define whether or not a gene is essential in *P. falciparum*. Indispensability of a gene is typically inferred from an inability to generate a knockout (43), and artificial maintenance of *P. falciparum* in culture may not be conducive to retrieval of a *Pf*ATPβ knockout. Indeed, the slightly reduced growth rate of *Pb*ATPβKO could suggest that recovery of a *P. falciparum* knockout may be difficult and that inducible knockdowns (43) should be explored.

The mitochondria of asexual blood-stage malaria parasites are unusual in that they typically lack mitochondrial cristae, which begin to develop only as the parasites differentiate into gametocytes (2, 13–15). The mitochondrial ATPase complex is responsible for generating the curvature of the cristae membranes (44, 45) so it is likely that up-regulation of ATPase in preparation for the sexual cycle is associated with development of mitochondrial cristae in malaria parasites. Indeed, transcriptomic and proteomic studies indicate up-regulation of mitochondrial enzymes during gametocytogenesis (12, 42, 46, 47), and *Pb*ATPβ protein (previous gene ID PB000896.02.0 and PB001169.01.0) in particular is far more abundant in female gametocytes than asexual blood stages (48). We observed distinct mitochondrial cristae in gametocytes in both parental and *Pb*ATPβKO parasites by transmission electron microscopy, suggesting that this subunit is not essential for cristae development during gametocytogenesis.

Given the dispensability of mitochondrial ATP synthase activity in asexual blood-stage *P. berghei* parasites shown here, and the fact that it is up-regulated for progression into the sexual cycle, we decided to examine the viability of our *Pb*ATPβKO mutant during the sexual stages and the insect phase of the parasite life cycle. The *Pb*ATPβKO produced marginally fewer gametocytes and exflagellation centers (sperm) than the parental line, but these differences were not statistically significant. We tracked fertilization and zygote differentiation into ookinetes in an in vitro system and found that the *Pb*ATPβKO parasites were only slightly, but statistically significantly, reduced in the ability to generate ookinetes. Intriguingly, the activation of female gametocytes, fertilization, and generation of ookinetes were drastically reduced for *Pb*ATPβKO parasites in vivo (i.e., within the mosquito gut). The mosquito gut is a harsh environment for parasites (11, 49), and the sole purpose of the highly motile ookinetes phase is to escape the gut and establish the new parasite generation in the insect hemocoel so it can produce sporozoites to accumulate in the salivary glands for transmission to new vertebrate hosts (35, 50). Rescue experiments demonstrated that as little as 10 h in the mosquito gut was detrimental to ookinete viability in our *Pb*ATPβKO parasites. We conclude that loss of mitochondrial ATP synthase function in *Pb*ATPβKO parasites renders them more vulnerable in the insect blood meal, compromising their ability to generate oocysts.

When we attempted to transmit *Pb*ATPβKO parasites through mosquitoes and back to naive mice, we observed a complete block in transmission. Given that ookinetes were not observed in vivo for *Pb*ATPβKO parasites, the absence of transmission was not surprising. We suspected that the gene deletion resulted in *Pb*ATPβKO female gametes, which carry the mitochondria in malaria parasites, with a fatal inadequacy for transmission. To test whether *Pb*ATPβKO is female infertile, we crossed our mutant with a male infertile line (*Pbs*48/45KO). P48/45 protein is a surface protein of both male and female malaria parasite gametes (39). Antibodies directed against P48/45 prevent zygote development, and P48/45 is under consideration as a target for a transmission-blocking vaccine to combat malaria (51). Disruption of the P48/45 gene results in a dramatic diminution of male-gamete fertility; the microgametes are unable to adhere to or penetrate macrogametes, and the number of oocysts produced is drastically reduced (39). Female fertility is retained in the *Pbs*48/45KO line (39). Our cross of *Pbs*48/45KO with *Pb*ATPβKO restored fertility in these two otherwise infertile lines. Ookinetes developed, oocysts formed on the mosquito midgut, and sporozoites accumulated in the mosquito salivary glands. Naive mice infected with these sporozoites developed blood-stage malaria infections in a normal time frame. We conclude that males from *Pb*ATPβKO successfully fertilized the females from *Pbs*48/45KO (Fig. S4). As a negative control, we crossed *Pb*ATPβKO parasites with a female infertile line, *Pbnek-4*$^{-}$, which resulted in no progeny and further confirmed that *Pb*ATPβKO is effectively female-sterile (Fig. S4).

Why is mitochondrial ATP synthase essential for female viability but not male fertility in rodent malaria parasites? Mitochondria are maternally inherited in malaria parasites, just as they are in most eukaryotes (32, 37, 38). The microgametes of *P. berghei*, and indeed those of all *Plasmodium* spp. examined, lack mitochondria (52) so lack of impact on male fertility by abrogation of *Pb*ATPβ makes sense. Indeed, proteomic analysis suggests that male gametocytes contain a lot less *Pb*ATPβ in comparison with female gametocytes (48). It is not known how malaria parasite microgametes obtain sufficient energy to swim (52), but even mammalian sperm, which do contain mitochondria, generate the bulk of their ATP by glycolysis (53); perhaps sufficient glucose persists in the blood meal to support malaria parasite microgamete motility and penetration of a macrogamete.

During female gametocytogenesis, the mitochondrion expands extensively (32), and changes in mitochondrial morphology and protein content indicate up-regulation of oxidative phosphorylation/chemiosmosis during the transition from the asexual blood-stage

lifestyle to sex in the mosquito gut (5, 12, 42, 46, 47). Our genetic dissection of the requirements for mitochondrial ATP synthesis suggest that successful activation of female gametes and subsequent production of durable ookinetes able to generate oocysts require mitochondrial ATP synthase whereas the asexual blood stages are apparently able to exist solely by glycolysis, albeit with a slightly reduced growth rate. Although the *Pb*ATPβKO line seemingly produces healthy ookinetes with normal mobility in vitro, they were not durable in vivo and were incapable of forming oocysts to extend the life cycle onwards. We conclude that adverse factors in the mosquito midgut compromise these parasites—with reduced ability to produce ATP—in some undetermined way. The block in fertility of *Pb*ATPβ prevents us from examining the role of mitochondrial ATP synthase in oocysts, sporozoites, and liver stages. Nevertheless, our data suggest that ATP synthase is unlikely to represent a good therapeutic drug target for blood-stage malaria. It could, however, be a target for transmission blocking if parasite ATPase activity can somehow be blocked in mosquito midguts.

Materials and Methods

Experimental Animals. Male Swiss Webster mice, between 4 and 6 wk old, were used in all experiments. Animals were sourced from either the Melbourne University Zoology animal facility or the Monash Animal Research Platform. All animal experiments were in accordance to the Prevention of Cruelty to Animals Act 1986 and the Prevention of Cruelty to Animals Regulations 2008 and reviewed and were permitted by the Melbourne University Animal Ethics Committee (Ethics ID 0810992.4, 1112043.1, and 1413078).

Parasites. *P. berghei* ANKA was used as a reference strain. *P. berghei* ANKA mutant line *Pbs*48/45KO (39) was provided by Andy Waters (University of Glasgow, Glasgow, Scotland). *Pb*nek-4^{-} (54) was provided by Oliver Billker (Wellcome Trust Sanger Institute, Hinxton, Cambridge, UK).

Bioinformatics Analysis. Bioinformatics analysis was done as described in *SI Materials and Methods*.

Generation of the *Pb*βL-GFP, the *Pb*ATPβKO, the *Pb*ATPβKO-YFP, and the *Pb*ATPβKO-GIMO-Tm Lines. Genetic modifications and confirmation of gene deletion were done as described in *SI Materials and Methods* and Table S1.

Observation of *Pb*βL-GFP Parasites in Blood and Mosquito Stages. *Pb*βL-GFP-infected mouse blood was incubated with 0.1 μg/mL Rhodamine 123 (Sigma-Aldrich) in culture media [RPMI (Invitrogen) plus 10% (vol/vol) FBS (Gibco)] at 37° C. Cells were then transferred into a Fluorodish Cell Culture Dish (Coherent Scientific) and imaged using an onstage incubator (INUBG2E-ONICS; Tokai Hit). To obtain mature schizonts, infected blood was incubated overnight in culture media at 37° C and a gas mixture (5% CO_2, 5% O_2, 90% N_2) before Rhodamine 123 staining and imaging as described above. For oocyst imaging, *A. stephensi* mosquitoes were infected with *Pb*βL-GFP and kept at 20° C for optimal parasite development. On days 7, 11, 14, and 17 after mosquito infection, mosquito midguts were dissected out, and images were captured at room temperature in PBS. For *Pb*βL-GFP sporozoites, salivary glands were dissected at day 22 after infection and disrupted to release the sporozoites. Images were also captured at room temperature in PBS. A Leica SP2 confocal microscope and Leica Confocal Software (version 2.61, build 1537) were used for imaging and 3D reconstructions. Further processing was done using Fiji (ImageJ 1.46a; Wayne Rasband, National Institutes of Health).

Reverse Transcriptase (RT)-PCR. RT-PCR was performed as described in *SI Materials and Methods* and Table S1.

Analysis of the *Pb*ATPβKO Line. The *Pb*ATPβKO parasites were checked for blood-stage growth, gametocyte formation, and exflagellation. Three sets of two mice were i.v. injected with 1×10^5 red blood cells infected with either *Pb*ANKA or *Pb*ATPβKO asexual stages. Blood smears from each mouse were prepared, and parasitemia and gametocyte levels (gametocytemia) were determined. *P* values were calculated using a paired *t* test. Between days 3 and 6 after infection, 1 μL of tail blood was taken and mixed with 100 μL of exflagellation media [RPMI (Invitrogen) supplemented with 10% FBS, pH 8.4]. After 15 min, exflagellation events per 1×10^5 red blood cells were counted by hemocytometer. *P* values were determined using a paired *t* test. For the growth competition experiment (Fig. 3*D*), 5×10^4 *Pb*ATPβKO-G6Tm parasites were mixed with 5×10^4 $PbGFP_{CON}$ parasites (33) and i.v. injected into eight mice. Between days 3 and day 7 after injection, blood samples were taken from the tail vein and analyzed for red and green fluorescence using a BD LSR Fortessa Cell Analyzer.

To analyze *Pb*ATPβKO parasites further, infected red blood cells were stained with Rhodamine 123 and imaged as described above. Transmission electron microscopy was performed to check mitochondrial morphology. Infected red blood cells where isolated using a Vario Macs Magnetic Cell Separator No. 1851 (Miltenyi Biotec) and subsequently fixed in 2.5% glutaraldehyde in 0.1 M cacodylate buffer for 2 h at 4 °C, followed by 1 h in 2% OsO_4, 1.5% potassium ferrocyanide in 0.15 M cacodylate, and 20 min at room temperature in 1% thyocarbohydrazide to allow additional osmium staining (55). Material was stained en bloc with 2% uranyl acetate and Walton's lead aspartate for maximum membrane contrast as described (55) before embedding in Durcupan Araldite embedding resin. Gametocytes were distinguished from asexual parasites by the presence of an inner membrane complex in the parasites (34).

For in vitro ookinete culture, mouse blood with high gametocyte levels was transferred into ookinete media [RPMI (GIBCO), 10% FBS (GIBCO), pH8.4] and incubated for 22 h at 21 °C. Cells were live immunolabeled (no fixation) with a monoclonal anti-Pbs28 antibody (1:500) (56) and an anti-mouse Alexa 488 (goat anti-mouse IgG, Alexa fluor R 488; Invitrogen) on ice for 1 h. Just before imaging, Hoechst 33342 (Sigma) was added to the cells at a final concentration of 5 μg/mL Activated females, zygotes, ookinetes, and aberrant-looking females were counted in a hemocytometer, and the composition of the culture was calculated in percent. Imaging was performed using a Leica SP2 confocal microscope and the Leica Confocal Software (version 2.61, build 1537). Further processing was done using Fiji (ImageJ 1.46a; Wayne Rasband, National Institutes of Health).

For the rescue experiment, mosquitoes where fed on *Pb*ANKA- and *Pb*ATPβKO-infected mice, presenting 20–30 exflagellations per 10^5 red blood cells. After mosquito feeding, mice were cardiac-bled, and blood was transferred into ookinete culture (see above) as a positive control. After 5 and 10 h, blood meals were dissected out of mosquito midguts (10 mosquitoes for each parasite line and each time point), gently homogenized using a sterile 1.5-mL pestle (Axygen), and transferred into ookinete culture media. Twenty-two hours after mosquito feeding, blood meals were dissected out (10 mosquitoes for each parasite line) and mixed with ookinete culture media as a negative control. All four different cultures were then stained with anti-Pbs28 as described above and checked for the presence of female developmental stages. This experiment was repeated five times.

For in vivo life cycle studies, mosquitoes were allowed to feed on *Pb*ANKA- and *Pb*ATPβKO-infected mice. Twenty-two hours later, midguts were dissected, and the blood meal was isolated. This blood meal was labeled with anti-Pbs28, and activated females, zygotes, ookinetes, and aberrant females were counted in a hemocytometer. Ten mosquito midgut contents were examined from three separate feeding experiments. Twelve days after mosquito infection, *Pb*ATPβKO-, *Pb*ATPβKO-YFP-, *Pb*ATPβKO-G6Tm-, and *Pb*ANKA-fed mosquito midguts were dissected and visually checked for the presence of oocysts. Twenty-two days after infection, salivary glands were dissected and checked for the presence of sporozoites. Finally, these mosquitoes were used in bite-back experiments with naive mice.

To check whether in vitro-produced *Pb*ATPβKO ookinetes could infect mosquitoes, artificial membrane feeding was performed with a concentration of ~3,000 *Pb*ATPβKO or *Pb*ANKA ookinetes per microliter of blood, diluted if necessary with uninfected mouse blood. After 12 d, midguts were checked for ookinetes; as well, salivary glands were checked for sporozoites after 22 d.

To compare ookinete motility of *Pb*ATPβKO parasites and WT parasites ($PbGFP_{CON}$), we performed Matrigel experiments as previously described (36). Briefly, a 1:1 mixture of ookinete cultures (mix of *Pb*ATPβKO and *Pb*GFPcon cultures) and Matrigel Matrix (Corning) was set onto a glass slide. The imaging (one frame every 10 s for 10 min) was done using a Leica SP2 confocal microscope and the Leica Confocal Software (version 2.61, build 1537). Manual tracking of ookinetes was done using Fiji (ImageJ 1.46a; Wayne Rasband, National Institutes of Health).

Crossing of Parasite Lines. Donor mice were preinfected with frozen stocks of parental *P. berghei* ANKA parasites and *Pb*ATPβKO and *Pbs*48/45KO (39) parasites. After 3–5 d, 5×10^5 parasites of each line from donor mice were injected i.v. into two mice, and a mixture of 2.5×10^5 *Pb*ATPβKO parasites and 2.5×10^5 *Pbs*48/45KO parasites was injected into a third mouse. When the tail-blood samples showed between 20 and 30 exflagellations per 1×10^5 red blood cells, mosquitoes were allowed to feed on the infected mice. Twelve

days later, midguts were dissected, and oocysts were counted. Twenty-two days after infection, salivary glands were dissected, and sporozoites were counted. The *Pb*ATPβKO-*Pbs*48/45KO mixed infected mosquitoes were allowed to feed on a naive mouse 22 d postinfection. A different batch of *Pb*ATPβKO-*Pbs*48/45KO mixed infected mosquitoes were dissected for sporozoites, and 3×10^4 sporozoites were i.v. injected into a naive mouse. After seven days, parasites were found in all mice. As a negative control for fertility complementation, we performed an equivalent cross between *Pb*ATPβKO and the female-deficient line *Pb*nek-4^{-} (40).

ACKNOWLEDGMENTS. We thank Andy Waters for the *Pbs*48/45KO and *Δp47* lines, Rebecca Stanaway for the pL0017-GFP$_{APICO}$ plasmid, and Bob Sinden for the anti-Pbs28 antibody. We thank Marcelo Jacobs-Lorena for teaching us to infect mosquitoes and Jake Baum for suggesting the cross. We thank the ImmunoID Flow Cytometry Facility at the University of Melbourne for assisting with the growth competition experiment. A.S. was supported by the Deutsche Forschungsgemeinschaft (DFG). We gratefully acknowledge a National Health and Medical Research Council Program Grant, an Australian Research Council Federation Fellowship, and an Australian Research Council Discovery Project (to G.I.M.).

1. Slavic K, et al. (2010) Life cycle studies of the hexose transporter of *Plasmodium* species and genetic validation of their essentiality. *Mol Microbiol* 75(6):1402–1413.
2. Bryant C, Voller A, Smith MJ (1964) The incorporation of radioactivity from [^{14}C] glucose into the soluble metabolic intermediates of malaria parasites. *Am J Trop Med Hyg* 13:515–519.
3. Scheibel LW, Miller J (1969) Glycolytic and cytochrome oxidase activity in *Plasmodia*. *Mil Med* 134(10):1074–1080.
4. Sherman IW, Ruble JA, Ting IP (1969) *Plasmodium lophurae*: (U-^{14}C)-glucose catabolism by free *Plasmodia* and duckling host erythrocytes. *Exp Parasitol* 25(1):181–192.
5. MacRae JI, et al. (2013) Mitochondrial metabolism of sexual and asexual blood stages of the malaria parasite *Plasmodium falciparum*. *BMC Biol* 11:67.
6. Scheibel LW, Pflaum WK (1970) Carbohydrate metabolism of *Plasmodium knowlesi*. *Comp Biochem Physiol B* 37:543–553.
7. Lunt SY, Vander Heiden MG (2011) Aerobic glycolysis: Meeting the metabolic requirements of cell proliferation. *Annu Rev Cell Dev Biol* 27:441–464.
8. Müller M, et al. (2012) Biochemistry and evolution of anaerobic energy metabolism in eukaryotes. *Microbiol Mol Biol Rev* 76(2):444–495.
9. Oliveira PL, Oliveira MF (2002) Vampires, Pasteur and reactive oxygen species: Is the switch from aerobic to anaerobic metabolism a preventive antioxidant defence in blood-feeding parasites? *FEBS Lett* 525(1-3):3–6.
10. Painter HJ, Morrisey JM, Mather MW, Vaidya AB (2007) Specific role of mitochondrial electron transport in blood-stage *Plasmodium falciparum*. *Nature* 446(7131):88–91.
11. Kuehn A, Pradel G (2010) The coming-out of malaria gametocytes. *J Biomed Biotechnol* 2010:976827.
12. Hall N, et al. (2005) A comprehensive survey of the *Plasmodium* life cycle by genomic, transcriptomic, and proteomic analyses. *Science* 307(5706):82–86.
13. Krungkrai J (2004) The multiple roles of the mitochondrion of the malarial parasite. *Parasitology* 129(Pt 5):511–524.
14. Aikawa M, Huff CG, Sprinz H (1969) Comparative fine structure study of the gametocytes of avian, reptilian, and mammalian malarial parasites. *J Ultrastruct Res* 26(3): 316–331.
15. Howells RE (1970) Mitochondrial changes during the life cycle of *Plasmodium berghei*. *Ann Trop Med Parasitol* 64(2):181–187.
16. Balabaskaran Nina P, et al. (2011) ATP synthase complex of *Plasmodium falciparum*: Dimeric assembly in mitochondrial membranes and resistance to genetic disruption. *J Biol Chem* 286(48):41312–41322.
17. Gardner MJ, et al. (2002) Genome sequence of the human malaria parasite *Plasmodium falciparum*. *Nature* 419(6906):498–511.
18. Mogi T, Kita K (2009) Identification of mitochondrial Complex II subunits SDH3 and SDH4 and ATP synthase subunits a and b in *Plasmodium* spp. *Mitochondrion* 9(6): 443–453.
19. Vaidya AB, Mather MW (2009) Mitochondrial evolution and functions in malaria parasites. *Annu Rev Microbiol* 63:249–267.
20. van Dooren GG, Stimmler LM, McFadden GI (2006) Metabolic maps and functions of the *Plasmodium* mitochondrion. *FEMS Microbiol Rev* 30(4):596–630.
21. Oppenheim RD, et al. (2014) BCKDH: The missing link in apicomplexan mitochondrial metabolism is required for full virulence of *Toxoplasma gondii* and *Plasmodium berghei*. *PLoS Pathog* 10(7):e1004263.
22. Torrentino-Madamet M, Desplans J, Travaillé C, James Y, Parzy D (2010) Microaerophilic respiratory metabolism of Plasmodium falciparum mitochondrion as a drug target. *Curr Mol Med* 10(1):29–46.
23. Sheiner L, Vaidya AB, McFadden GI (2013) The metabolic roles of the endosymbiotic organelles of *Toxoplasma* and *Plasmodium* spp. *Curr Opin Microbiol* 16(4):452–458.
24. Hino A, et al. (2012) Critical roles of the mitochondrial complex II in oocyst formation of rodent malaria parasite *Plasmodium berghei*. *J Biochem* 152(3):259–268.
25. Boysen KE, Matuschewski K (2011) Arrested oocyst maturation in *Plasmodium* parasites lacking type II NADH:ubiquinone dehydrogenase. *J Biol Chem* 286(37):32661–32671.
26. Walker JE (2013) The ATP synthase: The understood, the uncertain and the unknown. *Biochem Soc Trans* 41(1):1–16.
27. Boutry M, Douglas MG (1983) Complementation of a *Schizosaccharomyces pombe* mutant lacking the beta subunit of the mitochondrial ATPase by the ATP2 gene of *Saccharomyces cerevisiae*. *J Biol Chem* 258(24):15214–15219.
28. Boutry M, Goffeau A (1982) Alterations of the alpha or beta subunits of the mitochondrial ATPase in yeast mutants. *Eur J Biochem* 125(3):471–477.
29. Walker JE, Saraste M, Runswick MJ, Gay NJ (1982) Distantly related sequences in the alpha- and beta-subunits of ATP synthase, myosin, kinases and other ATP-requiring enzymes and a common nucleotide binding fold. *EMBO J* 1(8):945–951.
30. Bender A, van Dooren GG, Ralph SA, McFadden GI, Schneider G (2003) Properties and prediction of mitochondrial transit peptides from *Plasmodium falciparum*. *Mol Biochem Parasitol* 132(2):59–66.
31. van Dooren GG, et al. (2005) Development of the endoplasmic reticulum, mitochondrion and apicoplast during the asexual life cycle of *Plasmodium falciparum*. *Mol Microbiol* 57(2):405–419.
32. Okamoto N, Spurck TP, Goodman CD, McFadden GI (2009) Apicoplast and mitochondrion in gametocytogenesis of Plasmodium falciparum. *Eukaryot Cell* 8(1):128–132.
33. Franke-Fayard B, et al. (2004) A *Plasmodium berghei* reference line that constitutively expresses GFP at a high level throughout the complete life cycle. *Mol Biochem Parasitol* 137(1):23–33.
34. Dearnley MK, et al. (2012) Origin, composition, organization and function of the inner membrane complex of Plasmodium falciparum gametocytes. *J Cell Sci* 125(Pt 8): 2053–2063.
35. Kan A, et al. (2014) Computational analysis of *Plasmodium* ookinete motility suggests a critical role for cell shape in malaria parasite targeting and colonisation of the mosquito midgut. *Cell Micro* 16:734–750.
36. Moon RW, et al. (2009) A cyclic GMP signalling module that regulates gliding motility in a malaria parasite. *PLoS Pathog* 5(9):e1000599.
37. Creasey AM, et al. (1993) Uniparental inheritance of the mitochondrial gene cytochrome b in *Plasmodium falciparum*. *Curr Genet* 23(4):360–364.
38. Creasey A, et al. (1994) Maternal inheritance of extrachromosomal DNA in malaria parasites. *Mol Biochem Parasitol* 65(1):95–98.
39. van Dijk MR, et al. (2001) A central role for P48/45 in malaria parasite male gamete fertility. *Cell* 104(1):153–164.
40. van Dijk MR, et al. (2010) Three members of the 6-cys protein family of *Plasmodium* play a role in gamete fertility. *PLoS Pathog* 6(4):e1000853.
41. Bozdech Z, et al. (2003) Expression profiling of the schizont and trophozoite stages of *Plasmodium falciparum* with a long-oligonucleotide microarray. *Genome Biol* 4(2):R9.
42. Tarun AS, et al. (2008) A combined transcriptome and proteome survey of malaria parasite liver stages. *Proc Natl Acad Sci USA* 105(1):305–310.
43. Webster WA, McFadden GI (2014) From the genome to the phenome: Tools to understand the basic biology of *Plasmodium falciparum*. *J Eukaryot Microbiol* 61(6): 655–671.
44. Dudkina NV, Heinemeyer J, Keegstra W, Boekema EJ, Braun HP (2005) Structure of dimeric ATP synthase from mitochondria: An angular association of monomers induces the strong curvature of the inner membrane. *FEBS Lett* 579(25):5769–5772.
45. Strauss M, Hofhaus G, Schröder RR, Kühlbrandt W (2008) Dimer ribbons of ATP synthase shape the inner mitochondrial membrane. *EMBO J* 27(7):1154–1160.
46. Florens L, et al. (2002) A proteomic view of the *Plasmodium falciparum* life cycle. *Nature* 419(6906):520–526.
47. Young JA, Winzeler EA (2005) Using expression information to discover new drug and vaccine targets in the malaria parasite *Plasmodium falciparum*. *Pharmacogenomics* 6(1):17–26.
48. Khan SM, et al. (2005) Proteome analysis of separated male and female gametocytes reveals novel sex-specific *Plasmodium* biology. *Cell* 121(5):675–687.
49. Baton LA, Ranford-Cartwright LC (2012) Ookinete destruction within the mosquito midgut lumen explains *Anopheles albimanus* refractoriness to *Plasmodium falciparum* (3D7A) oocyst infection. *Int J Parasitol* 42(3):249–258.
50. Baton LA, Ranford-Cartwright LC (2005) How do malaria ookinetes cross the mosquito midgut wall? *Trends Parasitol* 21(1):22–28.
51. Kocken CH, et al. (1993) Cloning and expression of the gene coding for the transmission blocking target antigen Pfs48/45 of *Plasmodium falciparum*. *Mol Biochem Parasitol* 61(1):59–68.
52. Sinden RE, Canning EU, Spain B (1976) Gametogenesis and fertilization in *Plasmodium yoelii nigeriensis*: A transmission electron microscope study. *Proc R Soc Lond B Biol Sci* 193(1110):55–76.
53. Nascimento JM, et al. (2008) Comparison of glycolysis and oxidative phosphorylation as energy sources for mammalian sperm motility, using the combination of fluorescence imaging, laser tweezers, and real-time automated tracking and trapping. *J Cell Physiol* 217(3):745–751.
54. Reininger L, et al. (2005) A NIMA-related protein kinase is essential for completion of the sexual cycle of malaria parasites. *J Biol Chem* 280(36):31957–31964.
55. Wilke SA, et al. (2013) Deconstructing complexity: Serial block-face electron microscopic analysis of the hippocampal mossy fiber synapse. *J Neurosci* 33(2):507–522.
56. Paton MG, et al. (1993) Structure and expression of a post-transcriptionally regulated malaria gene encoding a surface protein from the sexual stages of *Plasmodium berghei*. *Mol Biochem Parasitol* 59(2):263–275.

Supporting Information

Sturm et al. 10.1073/pnas.1423959112

SI Materials and Methods

Bioinformatics Analysis. All *Plasmodium* sequences where retrieved from PlasmoDB (www.plasmodb.org/plasmo/). Other sequences were retrieved from UniProt (www.uniprot.org). Multiple sequence alignment was done using the Clustal Omega tool (www.ebi.ac.uk/Tools/msa/clustalo/), and mitochondrial targeting sequence prediction was done using the online tool MITOPROT (ihg.gsf.de/ihg/mitoprot.html).

Generation of the *Pb*βL-GFP, the *Pb*ATPβKO, the *Pb*ATPβKO-YFP, and the *Pb*ATPβKO-GIMO-Tm Lines. The first 240 bp of the *Plasmodium berghei* putative, mitochondrial ATP synthase β subunit (PBANKA_145030; www.plasmodb.org/plasmo/) were amplified by PCR using primers 21 and 42 (see Table S1 for primer sequences). The PCR product was cloned into the BamHI site of the pL0017-GFP_{APICO} plasmid, which contains the *Toxoplasma gondii* dihydrofolate reductase-thymidylate synthase (*Tg*DHFR/TS) resistance marker gene (1). The resulting plasmid, pL0017-$GFP_{\beta MITO}$ (Fig. 1*A*) ,was transfected into *P. berghei* ANKA parasites as previously described (2), giving rise to the *Pb*βL-GFP line.

To disrupt the ATP synthase, β subunit gene, we created a replacement plasmid using the vector pL0006 (MR4), which contains the resistance marker gene encoding for human dihydrofolate reductase (*h*DHFR). The 5′ and 3′ integration sequences for homologous recombination were amplified by PCR using primer combinations 27/29 (5′ integration sequence, 0.87 kb) and 30/31 (3′ integration sequence, 0.51kb) (see Table S1 for primer sequences). Integration sequences were cloned into pL0006 using the restriction enzymes XbaI/XhoI (5′ integration sequence) and StuI/SacII (3′ integration sequence). The resulting plasmid pL-β KO (Fig. 3*A*) was transfected into *P. berghei* ANKA parasites as previously described (2), giving rise to the ATPase β subunit knockout parasite line. Limiting dilution using 10 mice cloned this parasite line. Clone $C6_I$ (hereafter referred to as *Pb*ATPβKO) was used for all further analysis. The anticipated disruption of the β subunit gene was verified by PCR and Southern blot analysis using the DIG DNA Labeling and Detection Kit from Roche. For the latter, genomic DNA of the parental parasite line *Pb*ANKA and *Pb*ATPβKO was digested with the restriction enzymes NheI and XhoI, and the 5′ integration sequence, as well as a part of the *h*DHFR gene (using primer 63 and 64), was used as a probe. Using the 5′ integration sequence as a probe resulted in a 2.8-kb band for the WT locus and a 1.9-kb band for the *Pb*ATPβKO locus, indicating correct disruption of the β subunit locus (Fig. 3*B*). To verify our results, we produced a second knockout parasite line in an independent experiment. The knockout plasmid (pL-β KO–YFP) (Fig. S3*A*) was designed the same way as the pL-β KO plasmid, with the difference that the *h*DHFR marker gene was fused to the yellow fluorescent protein (YFP) gene. After transfection and cloning of the parasites, PCR and Southern blot analysis were performed as for the *Pb*ATPβKO line. The *Pb*ATPβKO-YFP parasite line also showed correct disruption of the β subunit. To perform the growth-competition experiment (Fig. 3*D*), we created a dtTomato (red fluorescent) version of *Pb*ATPβKO parasites using a modified version of the G6 parasites (3). In G6 parasites, the negative selection marker yFcu was used to recycle the positive selection marker dhfr, to create a nonpyrimethamine-resistant, GFP-expressing parasite. We swapped the GFP gene of the pBAT-SIL6 vector (3), which was used to create G6 parasites, with the dtTomato gene to create G6Tm, dtTomato-expressing, nonpyrimethamine-resistant parasites. After cloning, G6Tm parasites were transfected with the pL-β KO plasmid to create the *Pb*ATPβKO-G6Tm parasite line, which were cloned before use in the growth competition experiment.

Expression of the ATPase β subunit gene was assessed by Western blot analysis. Mouse blood [uninfected, infected (6% parasitemia)] with the parental *P. berghei* ANKA line, infected with either *Pb*ATPβKO or *Pb*ATPβKO-YFP), was passed through a column filled with CF11 powder (Whatman) to remove leukocytes. The resulting red blood cells were magnet-purified using a Vario Macs Magnetic Cell Separator No. 1851 (Miltenyi Biotec) and lysed with 0.15% saponin in PBS (5 min incubation at room temperature followed by three PBS washes). A 4–12% NuPage gradient gel (Invitrogen) was used to separate the proteins by SDS/PAGE. After protein transfer, the membrane was divided at the 62-kDa prestained marker band, and the lower section was probed with a commercial antibody raised against a synthetic peptide that is, according to the manufacturer, highly conserved in β subunits of known F-type ATP synthases from mitochondria, choloplasts, and most bacteria (dilution 1:5,000, AtpB; Agrisera,). The upper section of the membrane-carrying proteins of apparent mass greater than 62 kDa was probed with anti-Hsp70 antiserum (4).

Reverse Transcriptase (RT)-PCR. To detect ATP synthase β subunit transcripts, RNA was isolated from different life-cycle stages. To obtain asexual blood-stage *P. berghei* ANKA, infected mouse blood was magnet-purified, which removes gametocytes as well as very late asexual blood stages. For pure gametocyte samples, infected mice (~15% parasitemia) were treated with pyrimethamine (7 μg/mL in drinking water) for 48 h to kill off asexual blood stages, which was verified by Giemsa-stained blood smear. Twelve days after *Anopheles stephensi* infection, midguts were dissected out for oocyst RNA isolation. Eighteen days after infection, when sporogony was complete, midguts were again dissected out for the midgut sporozoite sample. Twenty-two days after infection, salivary-gland sporozoites were dissected out and used to infect human hepatoma (HepG2) cells (5), which were kept at 5% CO_2 and 37 °C in Advances MEM (GIBCO) supplemented with 10% FBS (GIBCO), 1% penicillin/streptomycin (HyClone 10.000 units/mL penicillin, 10,000 μg/mL streptomycin) and 2 mM L-Glutamine (HyClone). Samples were taken 24, 48, and 63 h after infection. RNA was isolated from all samples using the NucleoSpin RNA II Kit (Machery and Nagel) followed by DNaseI (Invitrogen) treatment. cDNA was made using the Omniscript RT Kit (Qiagen) and was used as template in a standard PCR to amplify parts of the ATP synthase β subunit (primers 7 and 8; 0.47 kb) and β-tubulin (primers 1 and 2; 0.42 kb) cDNA as control (see Table S1 for primer sequences). All RNA was checked for genomic DNA contamination by an RT (−) control.

1. Stanway RR, Witt T, Zobiak B, Aepfelbacher M, Heussler VT (2009) GFP-targeting allows visualization of the apicoplast throughout the life cycle of live malaria parasites. *Biol Cell* 101(7):415–430, and 5 pages following p 430.
2. Janse CJ, et al. (2006) High efficiency transfection of *Plasmodium berghei* facilitates novel selection procedures. *Mol Biochem Parasitol* 145(1):60–70.
3. Kooij TW, Rauch MM, Matuschewski K (2012) Expansion of experimental genetics approaches for *Plasmodium berghei* with versatile transfection vectors. *Mol Biochem Parasitol* 185(1):19–26.
4. Tsuji M, Mattei D, Nussenzweig RS, Eichinger D, Zavala F (1994) Demonstration of heat-shock protein 70 in the sporozoite stage of malaria parasites. *Parasitol Res* 80(1):16–21.
5. Hollingdale MR, Leland P, Schwartz AL (1983) In vitro cultivation of the exoerythrocytic stage of *Plasmodium berghei* in a hepatoma cell line. *Am J Trop Med Hyg* 32(4):682–684.

```
P.berghei                                       MNKFRFLKSLCSKKFANKINSQSLKTNCRFLSTT
M.musculus                                    MLSLVGRVASASASGALRGLSPSAALPQAQLLLRAA
A.thaliana          MASRRVLSSLLRSSSGRSAAKLGNRNPRLPSPSPARHAAPCSYLLGRVAEYATSSPASS

P.berghei           ENANLKKNINSSNIKGNVKGSANVGKISQVIGAVVDVEFQ--NTPPAILNALEVELDNKK
M.musculus          PAGVHPARDYAAQASAAPKAGTATGRIVAVIGAVVDVQFD--EGLPPILNALEVQGRDSR
A.thaliana          AAPSSAPAKDEGKKTYDYGGKGAIGRVCQVIGAIVDVRFEDQEGLPPIMTSLEVQDHPTR
                                          *    ****:***.*:  :  * *:.:***:   .:

P.berghei           LILEVAQHLGNKVVRTIAMDATDGLIRGQDVIDCGIPISVPVGKETLGRIMNVIGEPIDE
M.musculus          LVLEVAQHLGESTVRTIAMDGTEGLVRGQKVLDSGAPIKIPVGPETLGRIMNVIGEPIDE
A.thaliana          LVLEVSHHLGQNVVRTIAMDGTEGLVRGRKVLNTGAPITVPVGRATLGRIMNVLGEPIDE
                    *:***::***:..*******.*:**:**:.*:: * **.:***  ********:******

P.berghei           CGDIKSKKLLPIHRDPPLFTDQSTEPALLITGIKVVDLIAPYAKGGKIGLFGGAGVGKTV
M.musculus          RGPIKTKQFAPIHAEAPEFIEMSVEQEILVTGIKVVDLLAPYAKGGKIGLFGGAGVGKTV
A.thaliana          RGEIKTEHYLPIHRDAPALVDLATGQEILATGIKVVDLLAPYQRGGKIGLFGGAGVGKTV
                     * **:::  *** : * : : :.   :* ********:*** :****************

P.berghei           LIMELINNVAKKHGGYSVFAGVGERTREGNDLYHEMLTTGVIKKKKIKDNEYDFSGSKAA
M.musculus          LIMELINNVAKAHGGYSVFAGVGERTREGNDLYHEMIESGVINLKD--------ATSKVA
A.thaliana          LIMELINNVAKAHGGFSVFAGVGERTREGNDLYREMIESGVIKLGEK------QSESKCA
                    *********** ***:*******************:**: :***:  .       : ** *

P.berghei           LVYGQMNEPPGARARVALTGLTVAEYFRDEENQDVLLFVDNIYRFTQAGSEVSALLGRIP
M.musculus          LVYGQMNEPPGARARVALTGLTVAEYFRDQEGQDVLLFIDNIFRFTQAGSEVSALLGRIP
A.thaliana          LVYGQMNEPPGARARVGLTGLTVAEYFRDAEGQDVLLFIDNIFRFTQANSEVSALLGRIP
                    ****************.************ * ******:***:***** ***********

P.berghei           SAVGYQPTLATDLGALQERITTTKNGSITSVQAVYVPADDLTDPAPATTFSHLDATTVLS
M.musculus          SAVGYQPTLATDMGTMQERITTTKKGSITSVQAIYVPADDLTDPAPATTFAHLDATTVLS
A.thaliana          SAVGYQPTLASDLGALQERITTTKKGSITSVQAIYVPADDLTDPAPATTFAHLDATTVLS
                    **********:*:*::********:********:****************:*********

P.berghei           RSIAELGIYPAVDPLDSTSRMLTPDIVGVEQYEIARSIQQILQDYKSLQDIIAILGIDEL
M.musculus          RAIAELGIYPAVDPLDSTSRIMDPNIVGNEHYDVARGVQKILQDYKSLQDIIAILGMDEL
A.thaliana          RQISELGIYPAVDPLDSTSRMLSPHILGEEHYNTARGVQKVLQNYKNLQDIIAILGMDEL
                    * *:*****************:: *.*:* *:*: **.:*::**:**.*********:***

P.berghei           SEQDKLTVARARKVQRFLSQPFAVAEVFTGKPGRFVELDDTIKGFSELLKGNCDDIPEMA
M.musculus          SEEDKLTVSRARKIQRFLSQPFQVAEVFTGHMGKLVPLKETIKGFQQILAGEYDHLPEQA
A.thaliana          SEDDKLTVARARKIQRFLSQPFHVAEIFTGAPGKYVDLKENINSFQGLLDGKYDDLSEQS
                    **:*****:****:******** ***:***  *: * *.:.*:.*. :* *: *.: * :

P.berghei           FYMVGGLDEVKSKAIEMAKQM--
M.musculus          FYMVGPIEEAVAKADKLAEEHGS
A.thaliana          FYMVGGIDEVVAKAEKIAKESAA
                    ***** ::*. :** ::*::
```

Fig. S1. Multiple sequence alignment of ATP synthase β subunit proteins from *P. berghei*, *Mus musculus*, and *Arabidopsis thaliana*. Predicted mitochondrial targeting sequences are shown in gray. An asterisk indicates a site with a single, fully conserved residue; a colon indicates conservation between groups of strongly similar properties—scoring >0.5 in the Gonnet PAM 250 matrix; a period indicates conservation between groups of weakly similar properties—scoring ≤0.5 in the Gonnet PAM matrix.

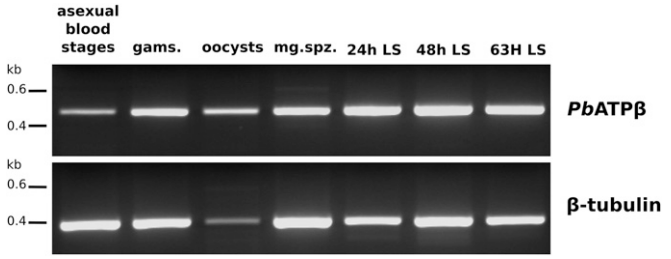

Fig. S2. The *Pb*ATPβ gene is expressed throughout the *P. berghei* life cycle. RT-PCR of the *Pb*ATPβ gene (*Upper*) and the *Pb*β-tubulin gene (*Lower*) at asexual blood stages, gametocytes (gams.), oocysts, midgut sporozoites (mg. spz.), and 24-, 48-, and 63-h liver stages (LS).

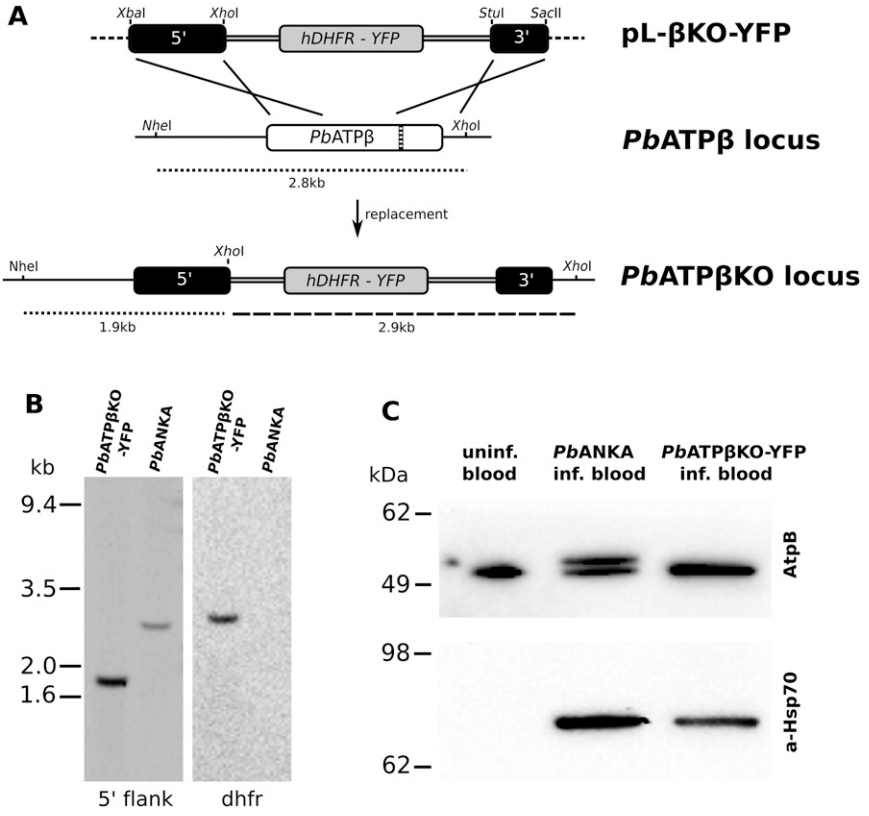

Fig. S3. Independent knockout of the *Pb*ATPβ gene locus to generate the *Pb*ATPβKO-YFP line, which also lacks *Pb*ATPβ protein production. (*A*) The plasmid pL-βKO-YFP with a selectable marker fused to the YFP gene (*h*DHFR-YFP) and flanked by 5′ and 3′ integration sequences amplified from the *Pb*ATPβ gene locus (5′ and 3′ black boxes) undergoes double cross-over, homologous recombination to delete a large section of the gene, including the catalytic domain (hatched bar) of *Pb*ATPβ. (*B*) Southern blot of genomic DNA from the *Pb*ATPβKO-YFP cloned line and the *Pb*ANKA parental line digested with NheI and XhoI and probed with the 5′ integration sequence (5′ flank) showing a single 1.9-kb band for *Pb*ATPβKO and the expected 2.8-kb band for parental WT parasites (*Pb*ANKA). Probing the same DNA with a hDHFR probe (dhfr) shows the expected single band at 2.9 kb and no band for *Pb*ANKA. (*C*) Western blot of uninfected mouse blood, *Pb*ANKA-infected mouse blood, and *Pb*ATPβKO-YFP-infected mouse blood, probed with the generic ATPβ protein antibody AtbP (*Upper*). The processed mouse ATPβ protein (50 kDa) is visible in uninfected mouse blood. A second, higher molecular mass band (54 kDa) is visible in mouse blood infected with WT parasites but not mouse blood infected with *Pb*ATPβKO-YFP parasites. Probing the upper part of the same membrane with a *P. berghei*-specific a-Hsp70 antibody (*Lower*) detected a band for *Pb*ANKA- and *Pb*ATPβKO-YFP-infected blood, confirming the presence of parasite material.

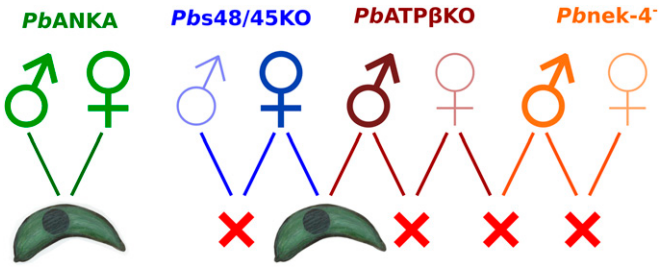

Fig. S4. Genetic crosses of PbATPβKO with male-deficient (Pbs48/45KO) or female-deficient (Pbnek-4^{-}) lines to more closely identify the life-cycle stage at which the fertility lesion in parasites deficient for mitochondrial ATP synthase activity occurs. Fertilization of a PbANKA female with a PbANKA male leads to normal development of a zygote (in green). Self-fertilization of the parasite lines Pbs48/45KO (blue), PbATPβKO (maroon), and Pbnek-4- (orange) is completely inhibited (red crosses). This sterility is due to infertile male gametocytes in Pbs48/45KO and infertile female gametocytes in Pbnek-4^{-} (indicated by faint symbols). By crossing two parasite lines with complementary phenotypes (Pbs48/45KO and PbATPβKO), fertility can be restored, resulting in the production of zygotes (purple).

Table S1. Primer sequences

Primer no.	Primer name	Sequence	Restriction site	Used for
1	Pb-tubulin-s	tggagcaggaaataactggg	—	RT-PCR control
2	Pb-tubulin-as	acctgacatagcggctgaaa	—	RT-PCR control
7	PbATPase-beta-s	ggaagtgcaaatgtcggtaaa	—	RT-PCR ATPase β subunit
8	PbATPase-beta-as	attggtttgtttggaggtgc	—	RT-PCR ATPase β subunit
21	PbATPase-beta-BamHI2-s	tgtGGATCCatgaataaatttcgatttttg	BamHI	pL0017-GFP$_{\beta\text{-mito}}$
27	PbATPbetaSCO-s	tgtCCCGGGtgaagagcttgtgctccaaa	XmaI	Integration seq.β KO construct
29	PbATPbetaDCO1-as	tgtCTCGAGccgcaacagttaagccagtt	XhoI	Integration seq.β KO construct
30	PbATPbetaDCO2-s	tgtAGGCCTcacctgatattgttggagtagagc	StuI	Integration seq.β KO construct
31	PbATPbetaDCO2-as	tgtCCGCGGagacattaaggaatgttgagcaa	SacII	Integration seq.β KO construct
42	PbATPase-beta-leader-BamHI-as	tgtGGATCCaattgctggtggcgtatttt	BamHI	pL0017-GFP$_{\beta\text{-mito}}$
63	hdhfr-s	ccgctcaggaacgaatttag	—	*h*DHFR probe
64	hdhfr-as	gtttaagatggcctgggtga	—	*h*DHFR probe

Primer sequences used for the generation of the different parasite lines and the performance of the reverse transcriptase (RT)-PCR. Capital letters indicate restriction sites, and dashes indicate the lack of restriction sites.

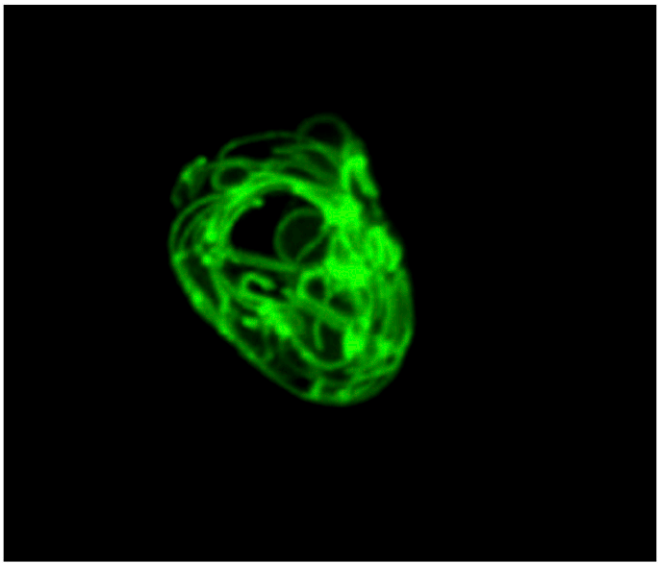

Movie S1. A 3D reconstruction of the mitochondrion in a *Pb*βL-GFP oocyst 11 d postinfection.

Movie S1

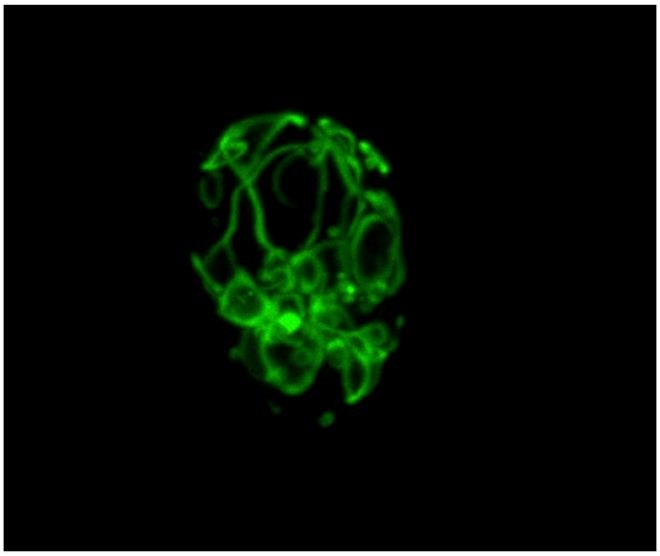

Movie S2. A 3D reconstruction of the mitochondrion in a *Pb*βL-GFP oocyst 14 d postinfection.

Movie S2

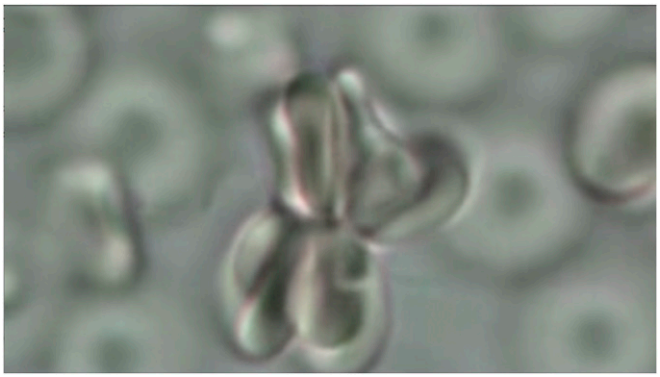

Movie S3. Recording of an exflagellation event of a *Pb*ATPβKO male gametocyte 15 min after transfer into exflagellation media. The male gametocyte has attached to uninfected red blood cells and is developing microgametes, which are seen as long sperm-like threads beating left and right to the red cell clump.

Movie S3